PHYSICAL REVIEW A **109**, 023106 (2024)

Energy-level-crossing study of forbidden transitions in highly charged ions with $(n = 4, 5)d^6$ and $(n = 4, 5)d^8$ configurations for making optical clocks

Yan-mei Yu[1,*] and B. K. Sahoo[2,†]
[1]Beijing National Laboratory for Condensed Matter Physics, Institute of Physics, Chinese Academy of Sciences, Beijing 100190, China
[2]Atomic, Molecular and Optical Physics Division, Physical Research Laboratory, Navrangpura, Ahmedabad 380009, India

(Received 26 July 2023; revised 3 November 2023; accepted 10 January 2024; published 5 February 2024)

Through the examination of energy level crossings among the fine-structure manifolds of the $(n = 4 - 5)d^6$ and $(n = 4 - 5)d^8$ configurations in a number of highly charged ions (HCIs), we identify forbidden transitions that can be suitable for making single-ion-based optical clocks. These clock transitions exhibit quality factors ranging between 10^{16} and 10^{18}, which are larger than most of the previously proposed HCI clock candidates. They also show high sensitivity to the temporal variation of the fine-structure constant and violation of the local Lorentz symmetry invariance. Detailed assessments of the Zeeman, Stark, black-body radiation, and electric quadrupole shifts associated with the above-proposed clock transitions are conducted to establish a typical order of magnitudes of their fractional uncertainties due to the systematic effects, which are found to be at the 10^{-19} level.

DOI: 10.1103/PhysRevA.109.023106

I. INTRODUCTION

A single highly charged ion (HCI) atomic clock, employing the magnetic dipole ($M1$) transition between the fine-structure (FS) splitting levels of the ground state in Ar^{13+}, has been achieved in the laboratory [1]. The motivation to use Ar^{13+} as an ultra-precise optical clock was driven by extensive studies carried out earlier [2–15]. Generally, HCIs exhibit enhanced sensitivity coefficients to variations of numerous fundamental physical constants and display minimal responses to external perturbations. These unique characteristics of the HCIs position them as valuable sensors and suitable candidates for testing several fundamental postulates of modern quantum mechanics, when employed as optical clocks [16–18].

The investigation of energy level-crossings (ELCs) in atomic systems is generally aimed at comprehending energy level shifts in the presence of external electromagnetic fields [19,20]. In the context of HCIs, this phenomenon pertains to the rearrangement of energy levels concerning the degree of ionization [21,22]. Through the analysis of ELCs, several HCIs have been proposed as potential candidates for atomic clocks, such as Ir^{17+} [23,24], Pr^{9+} [25], Cf^{16+} and Cf^{17+} [26,27], and Nd^{9+} [28], among others. Near ELCs, atomic transition frequencies may fall within the optical range, making them viable as frequency standards. Most of these HCIs possess multivalent outer f shells. Presently, studies have concentrated on the $4f$–$5s$ and $4f$–$5p$ transitions, for instance, in Ir^{17+} [24,29], Pr^{9+} [25], and Ho^{14+} [30], aiming at assessing their suitability for measuring optical clock frequencies.

The spectroscopic properties of HCIs within the d group find extensive applications in astronomy, plasma physics, and other phenomena involving high-temperature processes. The presence of open d shells leads to the existence of multiple fine-structure levels. Historically, optical forbidden transitions among these fine-structure levels have been extensively investigated [31–48]. Watanabe *et al.* investigated the visible and near-ultraviolet (UV) emission lines of titanium-like $3d^4$ HCIs in Ref. [33], while in Ref. [46], they determined energies and wavelengths of the $M1$ and electric quadrupole ($E2$) transitions for states with the $3d^n$ configurations in tungsten ions. Of particular interest are HCIs with d^6 and d^8 configurations due to their presence of hole states. These hole states are anticipated to exhibit very large relativistic sensitivity coefficients compared to particle-occupied states [22]. Previous studies suggested that HCIs with configurations such as p^4 [49,50], d^6 [51], and f^{12} [52] might host suitable forbidden transitions for optical-clock frequency measurements.

In this study, we explore the trends in energy levels within the low-lying states of heavier HCIs characterized by d^6 and d^8 configurations, utilizing relativistic atomic many-body methods. The d^6 open-shell configuration presents $^5D_{0,1,2,3,4}$ fine-structure states, while the d^8 configuration features $^3F_{4,3,2}$, $^1D_2$, and $^3P_{0,1,2}$ fine-structure states in their ground and low-lying excited states. Our investigation reveals that as the atomic number (Z) and ion charge (Z_{ion}) increase along the d^6 and d^8 isoelectronic sequences, ELCs manifest among these low-lying states. By tracking these patterns, we identify many long-lived states near these ELCs due to highly forbidden decay channels that open up the possibility of finding appropriate transitions to be considered for making optical clocks. We pin-point at least two feasible optical-accessible clock transitions in each type of the considered HCIs. Simultaneous operations of two clock transitions can be useful for minimizing systematic uncertainties in the measurement of

---

[*] ymyu@aphy.iphy.ac.cn

[†] bijaya@prl.res.in

the ratio of clock frequencies like in Yb^{+} [53]. Furthermore, a larger quality factor (Q) of a clock transition, defined as the ratio between the frequency and natural linewidth of the transition, implies a higher stability limit [54], resulting in a shorter averaging time to attain the desired systematic uncertainty in frequency measurements. The optical forbidden transitions found in the d^6 and d^8 configurations show larger Q values than the earlier-proposed HCI candidates based on the $M1$ transitions among the FS levels involving p orbitals [13–15]. These optical forbidden transitions also show reasonably enhanced sensitivity coefficients to the violation of local Lorentz symmetry invariance (LLI) and the variation of fine-structure constant (α). To evaluate the potentiality of the investigated HCIs with d^6 and d^8 configurations as high-precision clock candidates, we conduct detailed analyses on ions like Nd^{18+}, Ra^{14+}, Xe^{10+}, and Pb^{6+}, considering their clock-related properties and systematic effects. Our calculations include parameters, such as Landé's g_J factors, scalar (α_0^{E1}) and tensor (α_2^{E1}) electric dipole ($E1$) polarizabilities, electric quadrupole moments (Θ), as well as nuclear magnetic dipole (A_{hyp}) and electric quadrupole (B_{hyp}) hyperfine structure constants of the low-lying states of the considered HCIs.

II. COMPUTATIONAL METHODS

To assess the suitability of the HCIs with d^6 and d^8 configurations as clock candidates necessitates accurate data concerning their energies and other spectroscopic properties. While several d-group systems have previously undergone several theoretical investigations, information on the atomic data for the specified d^6 and d^8 systems of our interest remains limited. These HCIs, characterized by strong electronic correlation effects, pose challenges for accurate calculations using the existing many-body methods. To scrutinize the energy levels and properties of the HCIs relevant to this study, we have employthree distinct yet complementary *ab initio* calculation methods. The first method involves the combination of the relativistic configuration interaction (CI) method with many-body perturbation theory (MBPT), collectively referred to as the CI + MBPT method [55,56]. Here, the CI method accounts for valence-valence electron interactions, while the MBPT method addresses core-valence correlations. The second approach, known as the relativistic coupled-cluster (RCC) method, is considered as the gold standard of many-body theory. RCC calculations, restricted to the singles and doubles approximation (CCSD method), have been conducted exclusively for the d^8 configuration systems in the two-hole Fock-space formalism [57]. However, the Fock-space technique for computing wave functions of states with the d^6 configuration (four holes) remains to be very complex and has not been developed yet. Lastly, the relativistic multireference CI (MRCI) method, which addresses core-valence electronic correlations, has been employed [58–60]. Within this method, we truncate the CI method at both the singles and doubles approximation (CISD method) and the singles, doubles, and triples approximation (CISDT method).

We conduct a comparative analysis of the results obtained using all the three aforementioned many-body methods to assess the reliability of the recommended values. To carry out the calculations, we utilize single-particle matrix elements for various physical operators that are constructed locally as detailed in Ref. [61]. Each of the employed many-body methods is detailed below.

A. CI + MBPT method

We utilized the AMBIT code [62] to conduct the CI + MBPT calculations. The initial step in this method involves solving the Dirac-Hartree-Fock (DHF) wave function using the V^N potential, where N represents the number of electrons. We use the Dirac-Coulomb-Breit (DCB) Hamiltonian in these calculations. Within the AMBIT code, the emu-CI technique is adopted to reduce the size of the diagonalization matrix significantly, as detailed in Ref. [63]. All single and double excitations with the dominantly contributing configurations using $spdf$ orbitals are included, encompassing excitations within $n \leqslant 16$ and $l \leqslant 3$ where n denotes the principal quantum number and l signifies the orbital angular number. However, hole excitations within the core orbitals are omitted. In the MBPT method, we include all possible one-, two-, and three-body perturbative diagrams involving orbitals up to $30spdfg$ ($n \leqslant 30$, $l \leqslant 5$).

In our study, extending the basis size beyond $16spdf$ in the CI expansion and $30spdfg$ in the MBPT basis, along with the inclusion of orbitals with $l \leqslant 4$ in the CI expansion and those with $l \leqslant 5$ in the MBPT diagrams, resulted in a change in energy values less than 100 cm^{-1}. This observation indicates that our results from the CI + MBPT method achieve convergence with respect to the size of the basis, aligning with the convergence tests of the emu-CI technique previously demonstrated in the work by Geddes *et al.* [63].

B. CCSD method

The CCSD calculations are performed by employing the multireference valence-universal Fock-space approach, as discussed in Ref. [57], from the DIRAC program [64]. This code is based on the Dirac-Coulomb Hamiltonian, incorporating the Breit interaction partially at the self-consistent field (SCF) level through the Gaunt term, representing the spin-other orbit interaction. This results in the Dirac-Coulomb-Gaunt (DCG) Hamiltonian, presenting a slightly lower approximation compared to the DCB Hamiltonian. As the contribution from the retarded Breit interaction is deemed insignificant, comparing results between the DCB and DCG Hamiltonians remains acceptable. The initial DHF wave function is derived for the nd^{10} closed-shell configuration for the CCSD method. Subsequently, the desired fine-structure (FS) states with the nd^8 configurations are obtained by removing two electrons from the nd^{10} closed-shell configuration. To enhance the accuracy of the results, a correlation treatment is applied to all electrons, numbering 24 and 26 for the HCIs with $3d^6$ and $3d^8$ configurations, respectively, 42 and 44 for the HCIs with $4d^6$ and $4d^8$ configurations, respectively, and 74 and 76 for the ions with $5d^6$ and $5d^8$ configurations, respectively.

Furthermore, the calculations allowed singles and doubles excitations up to virtual orbitals with energies below 500 atomic units (a.u.). The impact of virtual orbitals with energies exceeding 500 a.u. on energy are tested to be within a few tens of cm^{-1} and hence are omitted here. The Dyall's triple-ξ

TABLE I. Energies of the low-lying excited states within the same fine-structure nd^6 and nd^8 manifolds are calculated for the Zn^{6+} ($3d^6$), Rb^{11+} ($3d^8$), Pd^{4+} ($4d^6$), Xe^{10+} ($4d^8$), and Pt^{4+} ($5d^6$) ions to carry out comparative analysis with the available experimental data (listed under "Literature" with associated error margins provided in parentheses from the respective references). These data are used to assess the accuracy of calculations performed using the CI + MBPT, CCSD, CISD, and CISDT methods. The "Diff" column presents the discrepancies between the values obtained via the "CISDT" method and those from the literature.

Ion	Level	Literature	AMBiT	CCSD	CISD	CISDT	Diff.
		Expt. [70,71]					
Zn^{6+}	$3d^6\ ^5D_4$	0	0		0	0	0
	$3d^6\ ^5D_3$	1567(±10)	1595		1559	1572(13)	0.3
	$3d^6\ ^5D_2$	2579(±10)	2633		2586	2584(2)	0.2
	$3d^6\ ^5D_1$	3230(±10)	3294		3239	3226(13)	−0.1
	$3d^6\ ^5D_0$	3542(±10)	3621		3557	3536(20)	−0.2
		Expt. [70,75]					
Rb^{11+}	$3d^8\ ^3F_4$	0	0	0	0	0	0.0
	$3d^8\ ^3F_3$	10 980(50)	10 980	10 772	11 276	11 284(9)	2.8
	$3d^8\ ^3F_2$	15 610(50)	15 796	15468	16 278	15 978(299)	2.4
	$3d^8\ ^1D_2$	34 020(50)	35 410	34 571	37 159	35 283(1876)	3.7
	$3d^8\ ^3P_1$	46 580(50)	48 774	46 748	50 590	48 642(1948)	4.4
	$3d^8\ ^3P_0$	47 220(50)	49 417	47 318	51 362	49 130(2231)	4.0
	$3d^8\ ^3P_2$	48 070(50)	49 654	48 731	52 037	50 034(2003)	4.1
		Expt. [74]					
Pd^{4+}	$4d^6\ ^5D_4$	0	0		0	0	0.0
	$4d^6\ ^5D_3$	2103.8(18.4)	2167		2106	2136(30)	1.6
	$4d^6\ ^5D_2$	3175.3(1.4)	3330		3259	3239(20)	2.0
	$4d^6\ ^5D_1$	3950(−9.4)	4141		4053	4027(26)	1.9
	$4d^6\ ^5D_0$	4306.4(−15.9)	4526		4429	4391(38)	2.0
		Expt. [70,72]					
Xe^{10+}	$4d^8\ ^3F_4$	0	0	0	0	0	0.0
	$4d^8\ ^3F_2$	13 140(17)	13 488	13 453	14 250	13 322(928)	1.4
	$4d^8\ ^3F_3$	15 205(16)	14 986	15 472	15 490	15 114(376)	−0.6
	$4d^8\ ^3P_2$	26 670(1)	26 934	27 172	27 884	26 812(1072)	0.5
	$4d^8\ ^3P_0$	32 210(2)	33 192	32 924	34 715	32 637(2078)	1.3
	$4d^8\ ^3P_1$	34 610(−2)	35 396	35 225	36 462	34 879(1583)	0.8
		Exp. [70,76]					
Pt^{4+}	$5d^6\ ^5D_4$	0	0		0	0	0.0
	$5d^6\ ^5D_2$	6026.34(−1.28)	6712		6720	6337(383)	5.2
	$5d^6\ ^5D_3$	7612.63(20.51)	7576		7210	7412(203)	−2.6
	$5d^6\ ^5D_0$	10817.6(−14.97)	11 378		11 216	10 893(323)	0.7
	$5d^6\ ^5D_1$	10 826.8(3.72)	11 085		10 797	10 756(41)	−0.7

correlation-consistent basis sets [65–68] are employed in the CCSD calculations.

C. MRCI method

The CISD and CISDT methods are implemented utilizing the KR-CI module [69] within the DIRAC package [64]. Initial DHF wave functions in this case are obtained using the average-of-configuration open-shell approximation for both the d^6 and d^8 configurations, employing the DCG Hamiltonian. In the DHF calculation, optimization of the Dirac spinors involved diagonalizing a Fock operator utilizing fractional occupations of $f = 6/10$ for the nd^6 configurations and $f = 8/10$ for the nd^8 spinors. This approach yields DHF states averaged over the $nd^{(6,8)}$ ground-state configurations, avoiding bias towards obtaining the final ground-state wave functions for both types of HCIs. These computations employ Dyall's triple-ξ correlation-consistent basis sets [65–68].

Subsequently, the CISD and CISDT calculations are performed to account for electron correlation effects within the atomic systems. Electron correlations are considered solely among electrons within the same principal quantum number, namely, the ns, np, and nd shells, with the other inner electrons held frozen. Excitations are permitted up to virtual orbitals with energy values of up to 10 a.u. The truncation of virtual orbitals ensures an adequate number for convergence. For instance, the MRCI correlation model space for the d^6 and d^8 configurations encompasses seven s, seven p, five d, six f, two g, and one h virtual functions. Triple excitations play significant roles in energy variations, amounting to about 1 to 6% deviation in the energies. Tests conducted using a smaller basis set in the singles and doubles approximation demonstrated significantly less influence from the inner-shell excitations and finite basis sets compared to triple excitations. Hence, our estimated uncertainty in the CISDT calculation should be in the 1 to 6% level, estimated

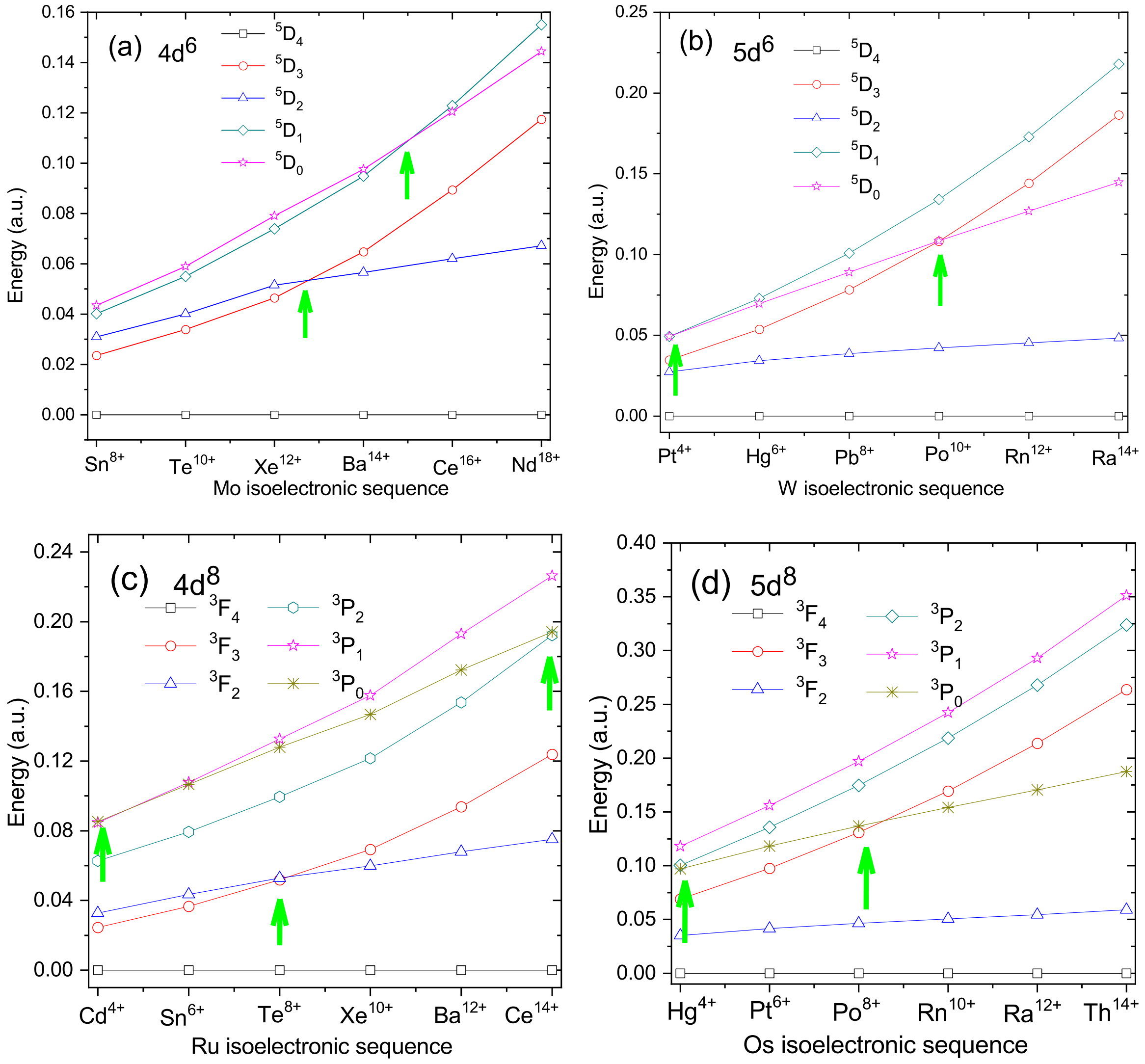

FIG. 1. Plots illustrating energy level crossings (ELCs) (indicated by arrows) in the HCIs with the $(n = 4, 5)d^{6,8}$ configurations across the (a) Mo-like, (b) W-like, (c) Ru-like, and (d) Os-like isoelectronic sequences. Energy values are presented in atomic units (a.u.).

by analyzing the differences between the CISD and CISDT results.

III. RESULTS AND DISCUSSION

A. Energies and ELCs

As shown in Table I, energies of several HCIs with d^6 and d^8 configurations, namely, the Cr-like Zn^{6+}, Fe-like Rb^{11+}, Mo-like Pd^{4+}, Ru-like Xe^{10+}, and W-like Pt^{4+} ions, are calculated using the CI + MBPT, CCSD, CISD, and CISDT methods. Experimental data for these HCIs are available in the National Institute of Science and Technology (NIST) atomic spectra database levels form, as well as from previous Refs. [70–78]. For brevity, we also give results for Xe^{10+} from our calculations in the Appendix and compare them with the data reported in Refs. [77,78]. They serve as examples of HCIs featuring optical-range excited states within the d^6 and d^8 fine-structure manifolds along each isoelectronic sequence. Although not all these ions are suitable for atomic clocks, the energy calculations for such ions can be considered for benchmarking accuracy of the calculated results for other HCIs obtained by employing the same many-body methods, where no data in the literature are available for the comparison.

From Table I, we find good agreement between the CI + MBPT results and the experimental data for the systems with $n = 3$. However, considerable disparities are evident for ions with $n = 4$ and $n = 5$. The CCSD results for the nd^8 ion show similar accuracy with the CI + MBPT results. In the case of heavier HCIs, such as Xe^{10+} ($4d^8$) and Pt^{4+} ($5d^6$), the CISDT results are found to be in better agreement with the experimental values than the CI + MBPT, CCSD, and CISD results. Thus, the results from the CISDT method, which should incorporate more physical effects through the triple excitations than the CISD method are considered the final calculated values. Nonetheless, a comparative analysis of the energy values from all three considered many-body methods helps us to test the reliability of the calculations in the considered HCIs with the d^6 and d^8 configurations.

TABLE II. The energy levels in cm^{-1} of the low-lying excited states above the ground state in the isoelectronic sequences of HCIs with the $(n = 4, 5)d^{6,8}$ configurations are determined using the CISDT method. The lower level that undergoes level crossing is shown in bold.

Mo-like with the $^5D_4$ ground state						
$4d^6$	Sn^{8+}	Te^{10+}	Xe^{12+}	Ba^{14+}	Ce^{16+}	Nd^{18+}
$^5D_3$	5161	7441	10 190	14 223	19 619	25 759
$^5D_2$	6792	8788	11 308	**12 412**	**13 609**	**14 735**
$^5D_1$	8817	12 062	16 215	20 807	26 969	34 017
$^5D_0$	9543	12 937	17 357	21 412	**26 444**	**31 706**
W-like with the $^5D_4$ ground state						
$5d^6$	Pt^{4+}	Hg^{6+}	Pb^{8+}	Po^{10+}	Rn^{12+}	Ra^{14+}
$^5D_3$	7412	11 792	17 160	23 749	31 649	40 925
$^5D_2$	**6637**	**7553**	**8488**	**9261**	**9944**	**10 617**
$^5D_1$	10 756	16 002	22 124	29 425	37 949	47 811
$^5D_0$	10 893	**15 271**	**19 546**	**23 814**	**27 867**	**31 777**
Ru-like with the $^3F_4$ ground state						
$4d^8$	Cd^{4+}	Sn^{6+}	Te^{8+}	Xe^{10+}	Ba^{12+}	Ce^{14+}
$^3F_3$	5378	8034	11 378	15 114	20 573	27 182
$^3F_2$	7189	9526	11 594	**13 322**	**14 933**	**16 471**
$^3P_2$	13 775	17 424	21 827	26 812	33 724	42 210
$^3P_1$	18 584	23 658	29 127	34 879	42 360	49 661
$^3P_0$	18 717	**23 402**	**28 074**	**32 637**	**37 821**	**42 610**
Os-like with the $^3F_4$ ground state						
$5d^8$	Hg^{4+}	Pb^{6+}	Po^{8+}	Rn^{10+}	Ra^{12+}	Th^{14+}
$^3F_3$	15 142	21 409	28 721	37 189	46 908	57 897
$^3F_2$	**7732**	**9104**	**10 170**	**11 096**	**11 960**	**12 953**
$^3P_2$	21 996	29 778	38 349	47 965	58 781	71 044
$^3P_1$	25 876	34 245	43 202	53 149	64 286	77 057
$^3P_0$	**21 296**	**25 957**	**30 041**	**33 816**	**37 407**	**41 165**

Now we intend to analyze ELCs in the FSs of the aforementioned isoelectronic sequence HCIs with nd^6 and nd^8 configurations for $n = 3$, 4, and 5 by increasing the ionization number Z_{ion}. Our focus primarily lies on the heavier HCIs, with moderate Z_{ion} values between 4 and 20, feasible for production using a table-top electron ion beam facility. Additionally, our concentration remains solely on the excited states falling within the 300 to 1000-nm range, accessible with available lasers. We exclude an investigation of radioactive HCIs possessing $(n = 6)d^{6,8}$ configurations due to their typically short half-lives, rendering them unsuitable for laboratory clock applications. Figure 1 displays the ground state and the low-lying excited states within the $(n = 4, 5)d^{6,8}$ fine-structure manifolds in each isoelectronic sequence. Figure 1 is plotted using the energy data obtained by the CISDT method, which is tabulated in Table II. The $(n = 3)d^{6,8}$ HCIs, devoid of ELCs, are not depicted. The Mo-like and W-like isoelectronic sequences exhibit $(n = 4, 5)d^6$ $^5D_4$ ground-state configurations and low-lying FS manifolds as ^5D_J with $J = 0, 1, 2, 3$. In Fig. 1(a), for smaller Z_{ion} values in the Mo-like isoelectronic sequences, like Sn^{8+} to Xe^{12+}, the FS level ordering progresses as $J = 4, 3, 2, 1, 0$. As Z_{ion} increases, the $^5D_3$ and $^5D_2$ levels interchange around Ba^{12+}, and the $^5D_0$ level shifts below the $^5D_1$ level around Ce^{16+}. Consequently, ELCs occur between the $J = 2$ and $J = 3$ levels and between the $J = 0$ and $J = 1$ levels, marked by arrows in Fig. 1(a) and highlighted in bold fonts in Table II. Similar ELC patterns are observed in the W-like isoelectronic sequences, as depicted in Fig. 1(b) and detailed in the table above. The Ru-like and Os-like isoelectronic sequences initially order levels as $^3F_2$, $^3F_1$, $^3F_0$, $^3P_2$, $^3P_1$, and $^3P_0$ for lower Z_{ion} values. However, their ordering changes from $^3F_3$ to $^3F_2$, from $^3P_1$ to $^3P_0$, and then from $^3P_0$ to $^3F_3$, indicated by arrows in Figs. 1(c) and 1(d). The energy data corresponding to each plot in Fig. 1 is detailed in Table II.

B. Identification of clock transitions

After comprehending the ELCs across different isoelectronic systems explored in this study, we can identify at least two clock transitions in each type of isoelectronic HCIs displaying ELCs. In HCIs with nd^6 configurations, the $^5D_4$–$^5D_2$ and $^5D_4$–$^5D_0$ ELC transitions correspond to the clock-I and clock-II transitions, respectively. Similarly, ELCs in the $^3F_4$–$^3F_2$ and $^3F_4$–$^3P_0$ transitions of the ions with the nd^8 configurations can be the clock-I and clock-II transitions, respectively. As these forbidden transitions are primarily guided by the $E2$ decay channel, they are expected to be relatively weak, resulting in considerably long lifetimes for the excited states. We can verify this by estimating the decay rates and lifetimes of these excited states. Table III lists a series of d^6 and d^8 HCIs featuring clock-I and clock-II transitions in the wavelength range of approximately 300 to 1000 nm. The table provides the respective λ values, Q values of the clock transitions, and associated lifetimes (τ) of the excited states for both clock transitions. It's notable that nearly all the listed HCIs exhibit sufficiently large τ and Q values, suggesting their suitability for making ultra-stable optical clocks.

C. Prospective of probing fundamental physics

The α-variation sensitivity coefficient of a transition is defined as

$$K_\alpha = 2(q_2 - q_1)/h\nu, \tag{1}$$

where $q_{1(2)}$ are α-variation sensitivity coefficients of the states associated with the transition $1 \rightarrow 2$, h is the Plank's constant, and ν is the transition frequency. The K_α values of the proposed clock transitions presented in Table III show that they are comparable or larger than the ^{171}Yb clock transitions [79].

Similarly, the LLI violating interaction Hamiltonian is given by [80]

$$H^{\text{LLI}} = -C_0^{(0)} \frac{\mathbf{p}^2}{2m_e} - C_0^{(2)} \frac{\mathbf{T}_0^{(2)}}{6m_e}, \tag{2}$$

where m_e is the mass of an electron, $C_0^{(0)}$ and $C_0^{(2)}$ are LLI violating coefficients, $\mathbf{p}$ is the momentum operator and $T_0^{(2)} = c\gamma_0(\gamma\mathbf{p} - 3\gamma_z p_z)$ with c being the speed of light, γ_0 and γ are the Dirac matrices [81]. Enhancement due to the kinetic energy of electrons are defined as $\Delta R = -(\langle J\|\mathbf{p}^2\|J\rangle_2 - \langle J\|\mathbf{p}^2\|J\rangle_1)/(2h\nu)$, and sensitivity needs to know the values of the reduced matrix elements of $T_0^{(2)}$. It was argued that to have an enhanced value of the LLI violation one needs to have long-living state (e.g., ground) with large value of the total electron momentum J ($J \geqslant 2$) and large values of the matrix

TABLE III. The estimated λ, τ, Q, ΔR, and $\langle J\|\mathbf{T}^{(2)}\|J\rangle$ values for the identified Clock-I and Clock-II transitions through ELC in a number of HCIs. The $\langle J\|\mathbf{T}^{(2)}\|J\rangle$ values for the ground and excited states of the Clock-I transition are only given for representation. See text for definitions of notations. $a[b]$ denotes $a \times 10^b$.

	Clock-I					Clock-II					$\langle J\|T^{(2)}\|J\rangle$(a.u.)	
Ions	λ (nm)	τ (s)	Q	K_α	ΔR	λ (nm)	τ (s)	Q	K_α	ΔR	ground	clock-I
						Mo-like ($4d^6$)						
Nd^{18+}	679	860	2.4[18]	0.1	0.8	315	138	8.2[17]	1.5	2.1	147	−47.5
						W-like ($5d^6$)						
Hg^{6+}	1255	1889	2.8[18]	0.4	1.7	655	505	1.5[18]	1.7	3.3	51.2	−14.6
Pb^{8+}	1178	1250	2.0[18]	0.5	1.2	512	107.0	3.9[17]	1.3	2.5	62.2	−20.8
Po^{10+}	1080	967	1.7[18]	−0.1	1.1	420	32.9	1.5[17]	1.1	2.1	73.5	−27.9
Rn^{12+}	1006	810	1.5[18]	−0.04	0.9	359	13.5	7.1[16]	0.9	1.8	85.5	−36.0
Ra^{14+}	942	690	1.3[18]	−0.01	0.9	315	6.8	4.1[16]	0.8	1.6	98.0	−44.7
						Ru-like ($4d^8$)						
Te^{8+}	863	772	1.7[18]	0.7	1.4	356	14	7.2[16]	0.5	1.3	−41.7	15.3
Xe^{10+}	761	480	1.2[18]	0.4	1.0	310	9.3	5.6[16]	0.5	1.3	−52.1	31.6
Ba^{12+}	670	285	8.0[17]	0.2	0.9	264	5.1	3.6[16]	0.5	1.2	−63.5	46.8
						Os-like ($5d^8$)						
Hg^{4+}	1293	643	9.4[18]	−0.3	1.8	470	8.2	3.3[16]	0.3	2.4	−27.8	23.4
Pb^{6+}	1098	393	6.7[18]	−0.3	1.5	385	3.8	1.9[16]	0.3	1.9	−36.7	31.5
Po^{8+}	983	311	6.0[18]	−0.1	1.2	333	2.3	1.3[16]	0.3	1.5	−46.7	40.3
Rn^{10+}	901	268	5.6[19]	−0.1	1.1	296	1.6	1.0[16]	0.3	1.4	−57.3	49.2

element for the LLI violating operator [81,82]. The clock-I transitions show somewhat big values of ΔR and $\langle J\|T^{(2)}\|J\rangle$ in Table III. Although these values are marginally smaller than the Yb^+ octupole transition and some f-shelled HCIs, they significantly surpass the clock transitions of Ca^+ [83,84] and Sr^+ [81], as illustrated in Table IV. This discussion underscores that the proposed clock transitions are not only suitable for making atomic clocks, but also highly sensitive in probing α variation and LLI violation.

TABLE IV. Differential relativistic R factors between the excited and ground states, i.e., $\Delta R \equiv \Delta R_{eg} = R_e - R_g$, and the $\langle J\|T^{(2)}\|J\rangle$ values (in a.u.) that are relevant for the LLI analysis in Nd^{18+} are given. They are compared with the values from other ions, which are also considered for similar studies.

Ions	States	ΔR	$\langle J\|T^{(2)}\|J\rangle$	Reference
Nd^{18+}	$4d^6\ {}^5D_4$	0	147	This work
	$4d^6\ {}^5D_2$	2.1	−47.5	This work
	$4d^6\ {}^5D_0$	0.8	0	This work
Os^{16+}	$4f^{12}5s^2\ {}^3H_6$	0	−299	[85]
	$4f^{12}5s^2\ {}^3F_4$	0.2	24	[85]
	$4f^{12}5s^2\ {}^3F_2$	2	122	[85]
Ir^{17+}	$4f^{13}5s\ {}^3F_4^o$	0	−283	[85]
	$4f^{12}5s^2\ {}^3H_6$	−30	−311	[85]
	$4f^{12}5s^2\ {}^3F_4$	−20	26	[85]
Pr^{9+}	$5p^2\ {}^3P_0$	0	0	[25]
	$5p4f\ {}^3G_3$	-	74.2	[25]
	$5p4f\ {}^3F_2$	-	54.8	[25]
Nd^{9+}	$(5p^24f)^o\ (J{=}5/2)$	-	73.67	[28]
	$(5p4f^2)^o\ (J{=}9/2)$	-	−85.20	[28]
Yb^+	$4f^{14}5d\ {}^2D_{5/2}$	1.48	12.08	[82]
	$4f^{13}6s^2\ {}^2F_{7/2}$	−1.9	−135.2	[82]
Ca^+	$3d\ {}^2D_{3/2}$	0.660(5)	7.09(12)	[83]
	$3d\ {}^2D_{5/2}$	0.660(5)	9.25(15)	[83]

D. Systematic effects

We proceed by discussing the primary systematic effects associated with the proposed clock transitions featuring the d^6 and d^8 configurations. Our examples include the Nd^{18+} with the $4d^6$ configuration, Ra^{14+} with the $5d^6$ configuration, Xe^{10+} with the $4d^8$ configuration, and Pb^{6+} with the $5d^8$ configuration, representing each configuration type. It is important to note that, for finite nuclear spin I, further energy splitting would occur, leading to many possible options for clock transitions. In some cases, it is useful in the sense that one can select a suitable combination of transitions for the experimental setup, but in other situations, they may complicate the experiment.

In view of this, it is necessary to learn about the orders of magnitudes of hyperfine splitting in the nonzero I systems. As is known, one can get to know the order of magnitudes of the hyperfine structures with the knowledge of the $A_{\rm hy}$ and $B_{\rm hf}$ values. For this purpose, we calculate the $A_{\rm hy}$ and $B_{\rm hf}$ values of ${}^{143}Nd^{18+}$, ${}^{223}Ra^{14+}$, ${}^{131}Xe^{10+}$, and ${}^{205}Pb^{6+}$, where the isotopes are either stable or have a longer lifetime. Generally, accurate calculations of the $A_{\rm hy}$ and $B_{\rm hf}$ values are very challenging because they are very sensitive to the behavior of the atomic wave functions in the nuclear region. In the considered HCIs, this challenge increases further as the d orbitals have a very small overlap with the nuclear region, and most of the contributions to these calculations arise from the s and p orbitals via the correlation effects, especially through the core-polarization effects.

Since there are no experimental data available, we make a comparison of the $A_{\rm hy}$ and $B_{\rm hf}$ values of the considered HCIs obtained by using the CI + MPBT, CISD, and CISDT methods in Table V. In the heavier ions like ${}^{223}Ra^{14+}$ and ${}^{205}Pb^{6+}$, the $A_{\rm hy}$ values obtained by using the CI + MBPT method show about 30% and 50% difference with those obtained by using the CISD and CISDT methods. To reduce uncertainties

TABLE V. The hyperfine structure constants A_{hf} and B_{hf} values of four representative HCIs evaluated using the CI + MBPT, CISD, and CISDT methods. The numbers in parentheses denote the error bars, which are estimated using the procedures discussed in the text. The nuclear magnetic dipole moment μ and the nuclear electric quadrupole moment $\mathcal{Q}_{\mathrm{nuc}}$ are in units of nuclear magneton μ_N and barn, respectively.

					A_{hf} (MHz)			B_{hf} (MHz)		
Ions	I	μ (μ_N)	$\mathcal{Q}_{\mathrm{nuc}}$ (barn)	states	CI+MBPT	CISD	CISDT	CI+MBPT	CISD	CISDT
^{143}Nd^{18+}	7/2	−1.065(5)	−0.61(2)	$4d^6\ ^5D_4$	−898	−935	−947(−7)	−4025	−4010	4008(−12)
				$4d^6\ ^5D_2$	−893	−929	−950(−9)	1268	1226	1254(−5)
^{223}Ra^{14+}	3/2	+0.271(2)	+1.25(7)	$5d^6\ ^5D_4$	494	350	351(−17)	6779	6591	6637(138)
				$5d^6\ ^5D_2$	491	349	346(−18)	−3020	−2936	−3013(−93)
^{131}Xe^{10+}	3/2	+0.6915(2)	−0.114(1)	$4d^8\ ^3F_4$	810	794	795(7)	222	223	224(−10)
				$4d^8\ ^3F_2$	999	1028	999(3)	−132	−134	−146(8)
^{205}Pb^{6+}	5/2	+0.7117(4)	+0.23(4)	$5d^8\ ^3F_4$	405	244	238(19)	−399	−411	−412(3)
				$5d^8\ ^3F_2$	447	375	373(8)	333	365	369(−4)

due to the use of the finite-size basis set, we repeat the CISD calculations using larger basis sets (dyall.cv4z for Nd and dyall.aae4z for Ra, Xe, and Pb) and check the consistency in the results. Variations in the results are accounted for in the error bars of the CCSDT results. Acomparison between results from the CI + MBPT and CISD methods and then between the results from the CISD and CISDT methods indicate that the A_{hy} values in the heavier Ra^{14+} and Pb^{6+} ions are overestimated in the CI + MBPT calculations. However, these values in other ions and the B_{hf} values from the CI + MPBT, CISD, and CISDT methods are almost in agreement.

To estimate the orders of shifts due to electric fields and BBR shifts in the above HCIs, we determine the scalar (α_0^{E1}) and tensor (α_2^{E1}) components of α^{E1}, and Θ values of the HCIs using the CISDT method in the finite-field (FF) approach. The errors in the α^{E1} and Θ values are estimated to be smaller than 5 to 10% due to the numerical factors, use of the finite-size basis set, truncation in the high-lying virtual orbitals and neglecting the electronic correlation from the deeper core and higher-level excitations. These error bars do not affect the objective of the intended study to identify the suitability of the considered HCIs as clock candidates.

As seen in Table VI, the differential $\delta\alpha_0^{E1}$ values of the proposed clock transitions are around 10^{-3}–10^{-4} a.u. Such small values mean that the fractional differential Stark shifts, $\delta E_{\mathrm{Stark}} = -\delta\alpha_0^{E1}\mathcal{E}^2/2$, of the clock transitions in the studied HCIs, for an input electric field strength $\mathcal{E}$=10 V/m, can be negligibly small. The differential BBR shift at the room temperature, $T = 300$ K, due to the $E1$ channel for a clock transition is estimated using the expression

$$\delta E_{\mathrm{BBR}}^{E1} = -\frac{1}{2}(831.9V/m)^2\left[\frac{T(K)}{300}\right]^4\delta\alpha_0^{E1}, \tag{3}$$

and found to be lower than or around 10^{-19} level in all the four HCIs. Similarly, the BBR shift due to other dominant $M1$ channels of the $|J\rangle$ state can be estimated using the formula

$$\Delta E_{\mathrm{BBR}}^{M1} = -\frac{\mu_0(K_BT)^2}{\pi^2(c\hbar)^3}\sum_{J'}\Bigg[|\langle J||O^{M1}||J'\rangle|^2\omega_{\eta\beta} \times \int_0^\infty d\omega\frac{\omega^3}{(\omega_{JJ'}^2-\omega^2)(\exp^{\hbar\omega/K_BT}-1)}\Bigg], \tag{4}$$

where μ_0, K_B, $\hbar$, and c are the magnetic permeability, Boltzmann's constant, Plank's constant, and speed of light, respectively, and $\langle J||O^{M1}||J'\rangle$ is the reduced $M1$ transition element. Then, the differential BBR shifts of the clock transitions, $\delta E_{\mathrm{BBR}}^{M1}$, are found to be slightly larger than the $E1$ BBR shifts at room temperature. However, due to the cryogenic environments, both of the $M1$ and $E1$ BBR shifts can be suppressed down to lower than 10^{-19} level.

The value of the electric field and the electric field gradients are chosen in this work referring to the experimental conditions that were reported in previous clock experiments. For example, in an electric field that an ion can feel of a few to a few hundred V/m [1]. In our work, we used a value of 10 V/m, which should be reasonable. In the paper of King *et al.*, the electric field gradient is reported to be 2×10^6 V/m^2. We use 10^8 V/m^2, which sounds reasonable. In a practical case, researchers can make conversions based on these reference data. By applying a factor of 10 to 20 due to the charge number, the frequency shift of energy levels caused by the intensity and gradient of the electric field might increase by one to two orders of magnitude. However, given the appropriate control over experimental parameters, the systematic shift should remain below 10^{-19}.

The electric quadrupole shift $\Delta E_\Theta = -\Theta\mathcal{E}_{zz}/2$, caused by the gradient of the applied electric field $\mathcal{E}_{zz}$ in the z direction, could be a major systematic effect in the atomic clock experiment. As shown in Table VI, despite one of the clock states $J = 0$ having $\Theta = 0$, the values of Θ for the $J = 4$ and $J = 2$ states are quite large, which can lead to significantly large electric quadrupole shifts in the $J = 4 - J = 2$ and $J = 4 - J = 0$ clock transitions. These shifts are estimated to be fractional shifts of the order of 10^{-14}–10^{-15} for an input value of $\mathcal{E}_{zz}$=10^8 V/m^2. Thus, it is necessary to use experimental techniques to reduce the differential quadrupole shifts in the proposed clock frequency measurements. This could be possible by averaging the frequency measurements over all magnetic projection components, which could nullify the electric quadrupole shifts. This can also help to cancel out the differential Stark shifts due to the tensor components of the $E1$ and $M1$ polarizabilities [86].

The first-order Zeeman shift of a clock transition is defined by $\delta E_{\mathrm{Zeem}}^{(1)} = \delta g_J\delta M\mu_B B$ for the external magnetic field B, Bohr magneton μ_B, δg_J is the differential Landé g_J factor, and δM is the differential M quantum number. Nullifying this

TABLE VI. Clock-related atomic properties and major fractional systematic effects of Nd^{18+} and Ra^{14+} that have the $^5D_4$ $(J = 4)$ ground state and two clock states, $^5D_2$ $(J = 2)$ and $^5D_0$ $(J = 0)$ and Xe^{10+} and Ra^{14+} that have the $^3F_4$ $(J = 4)$ ground state and two clock states, $^3F_2$ $(J = 2)$ and $^3P_0$ $(J = 0)$. Using the nuclear spin (I) values given in Table V, we consider the appropriate hyperfine structure levels to define the ground, clock-I, and clock-II states as $^5D_4$ $(F = 5/2)$, $^5D_2$ $(F = 3/2)$, and $^5D_0$ $(F = 7/2)$ for $^{143}\mathrm{Nd}^{18+}$, $^5D_4$ $(F = 5/2)$, $^5D_2$ $(F = 3/2)$, and $^5D_0$ $(F = 3/2)$ for $^{223}\mathrm{Ra}^{14+}$, $^3F_4$ $(F = 5/2)$, $^3F_2$ $(F = 3/2)$ and $^3P_0$ $(F = 3/2)$ for $^{131}\mathrm{Xe}^{10+}$ and $^3F_4$ $(F = 3/2)$, $^3F_2$ $(F = 3/2)$, and $^3P_0$ $(F = 5/2)$ for $^{205}\mathrm{Pb}^{6+}$. The $M1$ polarizability and fractional second-order Zeeman shifts are also evaluated for the corresponding hyperfine levels. Atomic units for electric dipole polarizability α can be converted to SI units [kHz $(\mathrm{kV\,cm}^{-1})^{-2}$] by multiplying with 0.248832, and the atomic units for the electric quadrupole moment Θ can be converted to SI units $[\mathrm{Hz}(\mathrm{V/m}^2)^{-1}]$ by multiplying with $6.770\,736 \times 10^{-7}$.

Items	Nd^{18+}	Ra^{14+}	Xe^{10+}	Pb^{6+}
g_J $(J = 4)$	1.4068	1.3199	1.242	1.2351
g_J $(J = 2)$	1.406	1.3293	0.9993	1.1171
Θ $(J = 4)$ (a.u.)	0.1088	0.2356	−0.1190	0.2827
Θ $(J = 2)$ (a.u.)	−0.0326	−0.1108	0.0674	0.2010
α_0^{E1} $(J = 4)$ (a.u.)	0.21956	0.6413	0.5817	2.4426
α_0^{E1} $(J = 2)$ (a.u.)	0.2202	0.6432	0.5824	2.4495
α_0^{E1} $(J = 0)$ (a.u.)	0.2196	0.6429	0.5826	2.4540
α_2^{E1} $(J = 4)$ (a.u.)	0.0046	0.0018	0.0036	0.0548
α_2^{E1} $(J = 2)$ (a.u.)	−0.0014	0.0003	−0.0057	−0.0291
α^{M1} $(J = 4)$ (a.u.)	-5.5×10^4	-2.7×10^4	-5.7×10^4	-5.5×10^4
α^{M1} $(J = 2)$ (a.u.)	-2.9×10^5	-7.5×10^4	-3.0×10^5	-6.4×10^4
α^{M1} $(J = 0)$ (a.u.)	-4.8×10^6	-6.3×10^5	-2.1×10^6	-5.3×10^5
$\alpha^{M1,\mathrm{hyp}}$ $(J = 4)$ (a.u.)	-1.4×10^6	1.2×10^6	-1.6×10^6	-1.2×10^7
$\alpha^{M1,\mathrm{hyp}}$ $(J = 2)$ (a.u.)	2.7×10^6	4.9×10^6	1.2×10^5	-1.6×10^7
ν $(J = 4 - J = 2)$ (a.u.)	0.0681	0.0484	0.0599	0.0464
ν $(J = 4 - J = 0)$ (a.u.)	0.1121	0.1448	0.1468	0.1276
$\delta E_{\mathrm{Stark}}/\nu$ $(J = 4 - J = 2)$	-2.0×10^{-24}	-7.3×10^{-24}	-2.2×10^{-24}	-2.8×10^{-23}
$\delta E_{\mathrm{Stark}}/\nu$ $(J = 4 - J = 0)$	-9.4×10^{-26}	-2.0×10^{-24}	-1.2×10^{-24}	-1.7×10^{-23}
$\delta E_{\mathrm{BBR}}^{E1}/\nu$ $(J = 4 - J = 2)$	-1.4×10^{-20}	-5.1×10^{-20}	-1.5×10^{-20}	-1.9×10^{-19}
$\delta E_{\mathrm{BBR}}^{E1}/\nu$ $(J = 4 - J = 0)$	-6.5×10^{-22}	-1.4×10^{-20}	-8.0×10^{-21}	-1.2×10^{-19}
$\delta E_{\mathrm{BBR}}^{M1}/\nu$ $(J = 4 - J = 2)$	-1.1×10^{-18}	1.1×10^{-19}	-9.0×10^{-20}	5.5×10^{-19}
$\delta E_{\mathrm{BBR}}^{M1}/\nu$ $(J = 4 - J = 0)$	-1.3×10^{-19}	5.4×10^{-20}	-1.6×10^{-20}	-3.2×10^{-19}
$\delta E_{\mathrm{Zeem}}^{(2)}/\nu$ $(J = 4 - J = 2)$	7.9×10^{-20}	2.2×10^{-20}	9.9×10^{-20}	2.9×10^{-21}
$\delta E_{\mathrm{Zeem}}^{(2)}/\nu$ $(J = 4 - J = 0)$	5.1×10^{-19}	9.5×10^{-20}	3.1×10^{-19}	8.4×10^{-20}
$\delta E_{\mathrm{Zeem,hyp}}^{(2)}/\nu$ $(J = 4 - J = 2)$	-1.4×10^{-18}	5.7×10^{-19}	-5.7×10^{-19}	2.2×10^{-18}
$\delta E_{\mathrm{Zeem,hyp}}^{(2)}/\nu$ $(J = 4 - J = 0)$	2.4×10^{-19}	3.0×10^{-19}	1.0×10^{-19}	-1.8×10^{-18}

shift involves measuring the transitions between all possible M components and averaging these measurements. However, the second-order Zeeman shift $\delta E_{\mathrm{Zeem}}^{(2)} = -\frac{1}{2}\delta\alpha^{M1}B^2$ can still be significant, wherein $\delta\alpha^{M1}$ is the differential value of α^{M1} between the clock states. We evaluate α^{M1} for the $|\gamma J M_J\rangle$ state as

$$\alpha^{M1}(J) = -\frac{2}{3(2J+1)}\sum_{J'}\frac{|\langle J||O^{M1}||J'\rangle|^2}{E_J - E_{J'}}. \tag{5}$$

We use the energies E and the reduced matrix element from the CISDT method to estimate the $\alpha^{M1}(J)$. For the HCIs with finite I values, we choose hyperfine levels with lower hyperfine angular momentum F to avoid complexities in the energy-level structures. In Table VI, we also list hyperfine-interaction-induced $M1$ polarizabilities $(\alpha^{M1,\mathrm{hyp}})$ for the $^{143}\mathrm{Nd}^{18+}$, $^{223}\mathrm{Ra}^{14+}$, $^{131}\mathrm{Xe}^{10+}$, and $^{205}\mathrm{Pb}^{6+}$ ions, considering the dominant contributions from the hyperfine manifolds of the same principle (n) and J states:

$$\alpha^{M1}(nIJF) = -\frac{2}{3(2F+1)}\sum_{F'}\frac{|\langle nIJF||O^{M1}||nIJF'\rangle|^2}{E_{nIJF} - E_{nIJF'}}, \tag{6}$$

and the reduced matrix element of O^{M1} is given by

$$\langle nIJF||O^{M1}||nIJF'\rangle = \mu_B\sqrt{J(J+1)(2J+1)(2F+1)} \times\sqrt{(2F'+1)}\begin{Bmatrix} I & J & F \\ 1 & F' & J \end{Bmatrix} g_J. \tag{7}$$

Here, the energies of the hyperfine levels are determined as

$$E_{nJF} = \frac{1}{2}A_{\mathrm{hf}}K + B_{\mathrm{hf}}\frac{(3/2)K(K+1) - 2I(I+1)J(J+1)}{4I(2I-1)J(2J-1)}, \tag{8}$$

where $K = F(F+1) - I(I+1) - J(J+1)$, utilizing the A_{hf} and B_{hf} values obtained from the CISDT method (refer to Table V). Considering an input value of $B = 5 \times 10^{-8}$T [87], the fractional shifts $\delta E^{(2)}_{\text{Zeem}}/\nu$ for all clock transitions are approximately at 10^{-19} level. However, the fractional shifts attributed to the second-order Zeeman effects in hyperfine structures may increase by one or two orders, but can be minimized by precisely calibrating the strength of the external magnetic field.

Based on the above analyses, it's evident that the fractional uncertainties resulting from major systematic effects such as the Zeeman, Stark, BBR, and electric quadrupole shifts can be effectively controlled at the 10^{-19} level, considering reasonable electric and magnetic field strengths. Notably, the $E2$ decay channel predominantly governs the proposed clock transitions. However, in certain scenarios, these transitions might occur through alternative channels. Among these, the $J = 4 - J = 0$ transition stands as highly forbidden, posing challenges for frequency measurement due to the potential requirement for strong external fields for its excitation. To address this, hyperfine quenching of forbidden transitions could prove instrumental in experiments concerning isotopes with finite I values. While they might decay to lower levels via the magnetic octupole ($M3$) and electric hexapole ($E4$) channels in ions with $I = 0$, their transition probabilities can be extremely small. For ions with $I \geqslant 1$, the $J = 4$ state can mix with the $J = 2$ state through the $E2$ component of the hyperfine interaction. This mixing leads to a finite transition probability to the ground state through the $E2$ channel, potentially presenting a more probable transition pathway compared to the $M3$ and $E4$ channels. It is necessary to further explore this transition channel in future studies.

IV. CONCLUSION

In summary, we identified a number of heavier highly charged ions by analyzing energy level-crossings within the ground d^6 and d^8 open-shell configurations, suitable for developing optical atomic clocks. They present at least two sets of clock transitions boasting quality factors around 10^{16-18} and fractional uncertainties from major systematic effects below the 10^{-19} level. These clock transitions also exhibit high sensitivity, making them ideal for investigating fundamental phenomena such as potential temporal variation of the fine-structure constant and local Lorentz symmetry invariance. To carry out these analyses, various spectroscopic properties of the considered ions are calculated by using three different relativistic many-body methods. These calculations can further serve as valuable guidelines to carry out future measurements using the undertaken ions and testing potentials of the employed methods.

ACKNOWLEDGMENTS

Y.Y. thanks K. Yao for sharing the work of the $3d$ ion EBIT spectroscopy. This work is supported by The National Key Research and Development Program of China (Grant No. 2021YFA1402104) and the project supported by the Space Application System of China Manned Space Program. B.K.S. acknowledges use of ParamVikram-1000 HPC of Physical Research Laboratory (PRL), Ahmedabad and his work at PRL is supported by the Department of Space, Government of India.

APPENDIX

In the Appendix, we have compared the results for the Ru-like Xe^{10+} ion from our calculations with the literature data in Table VII.

TABLE VII. Comparison of the calculated energies and transition probabilities of the excited states with the experimental results (Expt.) in Xe^{10+}. Here, the * symbol means the value is translated from the Ritz wavelength measurement and A_{ki} is the transition probability of the transition $k \to i$. The values under "This work" are obtained using the CISDT results. The values of A_{ki} under Refs. [77] and [78] are also the theoretical values obtained using the CI + MBPT method available in the AMBIT code and the relativistic many-body perturbation method implemented in the flexible atomic code (and references therein).

	Transition	Energy (eV)			A_{ki} (s^{-1})			Decay
Ion	($k \to i$)	Expt. [77]	Expt. [78] *	This work	[77]	[78]	This work	Channel
Xe^{10+}	$4d^8\ ^3P_1 - {}^3F_2$	2.6655150(26)	2.6619(38)	2.6751	47.8	42.70	46.5	$M1$
Xe^{10+}	$4d^8\ ^3P_2 - {}^3F_2$	1.68081600(90)	1.6774(30)	1.6725	35.8	30.90	35.7	$M1$
Xe^{10+}	$4d^8\ ^3F_3 - {}^3F_4$	1.8808627(14)	1.8851(25)	1.8738	88.4	78.70	87.7	$M1$
Xe^{10+}	$4d^8\ ^3F_2 - {}^3F_4$	1.6209726(34)		1.6517	0.002		0.0021	$E2$

[1] S. A. King, L. J. Spieß, P. Micke, A. Wilzewski, T. Leopold, E. Benkler, R. Lange, N. Huntemann, A. Surzhykov, V. A. Yerokhin, J. R. Crespo López-Urrutia, and P. O. Schmidt, Nature (London) **611**, 43 (2022).

[2] M. H. Prior, J. Opt. Soc. Am. B **4**, 144 (1987).

[3] D. J. Bieber, H. S. Margolis, P. K. Oxley, and J. D. Silver, Phys. Scr. **T73**, 64 (1997).

[4] I. Draganić, J. R. Crespo López-Urrutia, R. DuBois, S. Fritzsche, V. M. Shabaev, R. S. Orts, I. I. Tupitsyn, Y. Zou, and J. Ullrich, Phys. Rev. Lett. **91**, 183001 (2003).

[5] I. I. Tupitsyn, V. M. Shabaev, J. R. Crespo López-Urrutia, I. Draganić, R. S. Orts, and J. Ullrich, Phys. Rev. A **68**, 022511 (2003).

[6] M. G. Kozlov, V. A. Korol, J. C. Berengut, V. A. Dzuba, and V. V. Flambaum, Phys. Rev. A **70**, 062108 (2004).

[7] A. Lapierre, U. D. Jentschura, J. R. Crespo López-Urrutia, J. Braun, G. Brenner, H. Bruhns, D. Fischer, A. J. González Martínez, Z. Harman, W. R. Johnson, C. Keitel, V. Mironov, C. J. Osborne, G. Sikler, R. Soria Orts, V. Shabaev, H. Tawara, I. I. Tupitsyn, J. Ullrich, and A. Volotka, Phys. Rev. Lett. **95**, 183001 (2005).

[8] I. I. Tupitsyn, A. V. Volotka, D. A. Glazov, V. M. Shabaev, G. Plunien, J. R. Crespo López-Urrutia, A. Lapierre, and J. Ullrich, Phys. Rev. A **72**, 062503 (2005).

[9] A. Lapierre, J. R. Crespo López-Urrutia, J. Braun, G. Brenner, H. Bruhns, D. Fischer, A. J. González Martínez, V. Mironov, C. Osborne, G. Sikler, R. Soria Orts, H. Tawara, J. Ullrich, V. M. Shabaev, I. I. Tupitsyn, and A. Volotka, Phys. Rev. A **73**, 052507 (2006).

[10] R. Soria Orts, Z. Harman, J. R. Crespo López-Urrutia, A. N. Artemyev, H. Bruhns, A. J. González Martínez, U. D. Jentschura, C. H. Keitel, A. Lapierre, V. Mironov, V. M. Shabaev, H. Tawara, I. I. Tupitsyn, J. Ullrich, and A. V. Volotka, Phys. Rev. Lett. **97**, 103002 (2006).

[11] Z. Harman, U. D. Jentschura, C. H. Keitel, A. Lapierre, R. Soria Orts, J. R. Crespo López-Urrutia, H. Tawara, J. Ullrich, A. N. Artemyev, I. I. Tupitsyn, A. V. Volotka, and V. M. Shabaev, J. Phys.: Conf. Ser. **58**, 133 (2007).

[12] V. Mäckel, R. Klawitter, G. Brenner, J. R. Crespo López-Urrutia, and J. Ullrich, Phys. Rev. Lett. **107**, 143002 (2011).

[13] V. I. Yudin, A. V. Taichenachev, and A. Derevianko, Phys. Rev. Lett. **113**, 233003 (2014).

[14] Y. M. Yu and B. K. Sahoo, Phys. Rev. A **94**, 062502 (2016).

[15] Y. M. Yu and B. K. Sahoo, Phys. Rev. A **99**, 022513 (2019).

[16] M. S. Safronova, D. Budker, D. DeMille, Derek F. Jackson Kimball, A. Derevianko, and C. W. Clark, Rev. Mod. Phys. **90**, 025008 (2018).

[17] M. G. Kozlov, M. S. Safronova, J. R. Crespo López-Urrutia, and P. O. Schmidt, Rev. Mod. Phys. **90**, 045005 (2018).

[18] Y. M. Yu, B. K. Sahoo, and B. B. Suo, Front. Phys. **11**, 1104848 (2023).

[19] R. T. Robiscoe, Phys. Rev. **138**, A22 (1965).

[20] J. S. Levine, P. A. Bonczyk, and A. Javan, Phys. Rev. Lett. **22**, 267 (1969).

[21] J. C. Berengut, V. A. Dzuba, and V. V. Flambaum, Phys. Rev. Lett. **105**, 120801 (2010).

[22] J. C. Berengut, V. A. Dzuba, V. V. Flambaum, and A. Ong, Phys. Rev. A **86**, 022517 (2012).

[23] J. C. Berengut, V. A. Dzuba, V. V. Flambaum, and A. Ong, Phys. Rev. Lett. **106**, 210802 (2011).

[24] A. Windberger, J. R. Crespo López-Urrutia, H. Bekker, N. S. Oreshkina, J. C. Berengut, V. Bock, A. Borschevsky, V. A. Dzuba, E. Eliav, Z. Harman, U. Kaldor, S. Kaul, U. I. Safronova, V. V. Flambaum, C. H. Keitel, P. O. Schmidt, J. Ullrich, and O. O. Versolato, Phys. Rev. Lett. **114**, 150801 (2015).

[25] H. Bekker, A. Borschevsky, Z. Harman, C. H. Keitel, T. Pfeifer, P. O. Schmidt, J. R. Crespo López-Urrutia, and J. C. Berengut, Nat. Commun. **10**, 5651 (2019).

[26] J. C. Berengut, V. A. Dzuba, V. V. Flambaum, and A. Ong, Phys. Rev. Lett. **109**, 070802 (2012).

[27] S. G. Porsev, U. I. Safronova, M. S. Safronova, P. O. Schmidt, A. I. Bondarev, M. G. Kozlov, I. I. Tupitsyn, and C. Cheung, Phys. Rev. A **102**, 012802 (2020).

[28] Y. M. Yu, P. Duo, S. L. Chen, B. Arora, H. Guan, K. Gao, and J. Chen, Atoms **10**, 123 (2022).

[29] C. Cheung, M. S. Safronova, S. G. Porsev, M. G. Kozlov, I. I. Tupitsyn, and A. I. Bondarev, Phys. Rev. Lett. **124**, 163001 (2020).

[30] T. Nakajima, K. Okada, M. Wadac, V. A. Dzuba, M. S. Safronova, U. I. Safronova, N. Ohmae, H. Katori, and N. Nakamura, Nucl. Instrum. Methods Phys. Res., Sect. B **408**, 118 (2017).

[31] S. Suckewer, E. Hinnov, S. Cohen, M. Finkenthal, and K. Sato, Phys. Rev. A **26**, 1161 (1982).

[32] C. A. Morgan, F. G. Serpa, E. Takacs, E. S. Meyer, J. D. Gillaspy, J. Sugar, J. R. Roberts, C. M. Brown, and U. Feldman, Phys. Rev. Lett. **74**, 1716 (1995).

[33] H. Watanabe, D. Crosby, F. J. Currell, T. Fukami, D. Kato, S. Ohtani, J. D. Silver, and C. Yamada, Phys. Rev. A **63**, 042513 (2001).

[34] R. Doron and U. Feldman, Phys. Scr. **64**, 319 (2001).

[35] N. Kimura, Priti, Y. Kono, P. Pipatpakorn, K. Soutome, N. Numadate, S. Kuma, T. Azuma, and N. Nakamura, Commun. Phys. **6**, 8 (2023).

[36] J. R. Crespo López-Urrutia, P. Beiersdorfer, K. Widmann, and V. Decaux, Can. J. Phys. **80**, 1687 (2002).

[37] D. Osin, J. D. Gillaspy, J. Reader, and Y. Ralchenko, Eur. Phys. J. D **66**, 286 (2012).

[38] T. Lennartsson, J. Clementson, and P. Beiersdorfer, Phys. Rev. A **87**, 062505 (2013).

[39] A. Windberger, F. Torretti, A. Borschevsky, A. Ryabtsev, S. Dobrodey, H. Bekker, E. Eliav, U. Kaldor, W. Ubachs, R. Hoekstra, J. R. Crespo López-Urrutia, and O. O. Versolato, Phys. Rev. A **94**, 012506 (2016).

[40] F. Torretti, A. Windberger, A. Ryabtsev, S. Dobrodey, H. Bekker, W. Ubachs, R. Hoekstra, E. V. Kahl, J. C. Berengut, J. R. Crespo López-Urrutia, and O. O. Versolato, Phys. Rev. A **95**, 042503 (2017).

[41] R. Silwal, Dipti, E. Takacs, J. M. Dreiling, S. C. Sanders, A. C. Gall, B. H. Rudramadevi, J. D. Gillaspy, and Y. Ralchenko, J. Phys. B **54**, 245001 (2021).

[42] C. Y. Zhang, J. Q. Li, K. Wang, R. Si, M. Godefroid, P. Jönsson, J. Xiao, M. F. Gu, and C. Y. Chen, Phys. Rev. A **105**, 022817 (2022).

[43] Z. C. He, J. Meng, Y. J. Li, F. S. Jia, N. Khan, B. Niu, L. Y. Huang, Z. M. Hu, J. G. Li, J. G. Wang, Y. M. Zou, B. R. Wei, and K. Yao, J. Quant. Spectrosc. Radiat. Transfer **288**, 108276 (2022).

[44] F. Junyu, Z. Jiang, Y. Qian, J. Liu, P. Xu, L. Huang, Z. He, Y. Zou, J. Li, C. Chen, and K. Yao, Atoms **10**, 154 (2022).

[45] Y. Ralchenko, I. N. Draganić, D. Osin, J. D. Gillaspy, and J. Reader, Phys. Rev. A **83**, 032517 (2011).

[46] M. S. Safronova, U. I. Safronova, S. G. Porsev, M. G. Kozlov, and Yu. Ralchenko, Phys. Rev. A **97**, 012502 (2018).

[47] G. C. Rodrigues, P. Indelicato, J. P. Santos, P. Patté, and F. Parente, At. Data Nucl. Data Tables **86**, 117 (2004).

[48] S. S. Churilov and A. N. Ryabtsev, Phys. Scr. **73**, 614 (2006).

[49] Y. M. Yu and B. K. Sahoo, Phys. Rev. A **97**, 041403(R) (2018).

[50] S. O. Allehabi, S. M. Brewer, V. A. Dzuba, V. V. Flambaum, and K. Beloy, Phys. Rev. A **106**, 043101 (2022).

[51] Chunhai Lyu, Christoph H. Keitel, and Zoltán Harman, arXiv:2305.09603.

[52] V. A. Dzuba, A. Derevianko, and V. V. Flambaum, Phys. Rev. A **86**, 054501 (2012).

[53] R. Lange, N. Huntemann, J. M. Rahm, C. Sanner, H. Shao, B. Lipphardt, Chr. Tamm, S. Weyers, and E. Peik, Phys. Rev. Lett. **126**, 011102 (2021).

[54] A. D. Ludlow, M. M. Boyd, and J. Ye, E. Peik, and P. O. Schmidt, Rev. Mod. Phys. **87**, 637 (2015).

[55] V. A. Dzuba, V. V. Flambaum, and M. G. Kozlov, Phys. Rev. A **54**, 3948 (1996).

[56] J. C. Berengut, V. V. Flambaum, and M. G. Kozlov, Phys. Rev. A **73**, 012504 (2006).

[57] L. Visscher, E. Eliav, and U. Kaldor, J. Chem. Phys. **115**, 9720 (2001).

[58] T. Fleig, J. Olsen, and C. M. Marian, J. Chem. Phys. **114**, 4775 (2001).

[59] T. Fleig, J. Olsen, and L. Visscher, J. Chem. Phys. **119**, 2963 (2003).

[60] T. Fleig, H. J. A. Jensen, J. Olsen, and L. Visscher, J. Chem. Phys. **124**, 104106 (2006).

[61] H. X. Liu, Y. M. Yu, B. B. Suo, Y. Liu, and B. K. Sahoo, Phys. Rev. A **108**, 032804 (2023).

[62] E. V. Kahl and J. C. Berengut, Comput. Phys. Commun. **238**, 232 (2019).

[63] A. J. Geddes, D. A. Czapski, E. V. Kahl, and J. C. Berengut, Phys. Rev. A **98**, 042508 (2018).

[64] CIRAC, a relativistic *ab initio* electronic structure program, release DIRAC22 (2022), written by H. J. Aa. Jensen *et al.* (available at http://dx.doi.org/10.5281/zenodo.6010450, see also http://www.diracprogram.org).

[65] K. G. Dyall, P. Tecmer, and A. Sunaga, J. Chem. Theory Comput. **19**, 198 (2023).

[66] K. G. Dyall, Theor. Chem. Acc **108**, 335 (2002).

[67] K. G. Dyall, Theor. Chem. Acc. **115**, 441 (2006).

[68] A. S. P. Gomes, K. G. Dyall, and L. Visscher, Theor. Chem. Acc. **127**, 369 (2010) All dyall basis sets available from the Dirac web site, http://dirac.chem.sdu.dk.

[69] S. Knecht, H. J. A. Jensen, and T. Fleig, J. Chem. Phys. **128**, 014108 (2008).

[70] A. Kramida, Y. Ralchenko, J. Reader, and NIST ASD Team, https://physics.nist.gov/asd.

[71] J. Sugar and A. Musgrove, J. Phys. Chem. Ref. Data **24**, 1803 (1995).

[72] S. S. Churilov, Y. N. Joshi, J. Reader, and R. R. Kildiyarova, Phys. Scr. **70**, 126 (2004).

[73] B. Edlén, Phys. Scr. **T8**, 5 (1984).

[74] A. J. J. Raassen and Th. A. M. van Kleef, Physica C **142**, 359 (1986).

[75] J. E. Sansonettia, J. Phys. Chem. Ref. Data **35**, 301 (2006).

[76] V. I. Azarov and R. R. Gayasovb, At. Data Nucl. Data Tables **108**, 154 (2016).

[77] N. H. Rehbehn, M. K. Rosner, J. C. Berengut, P. O. Schmidt, T. Pfeifer, M. F. Gu, and J. R. Crespo López-Urrutia, Phys. Rev. Lett. **131**, 161803 (2023).

[78] B. Niu, Y. Zhang, J. Chen, S. Meng, K. Yao, Y. Zou, J. Li, Z. He, and J. Meng, Can. J. Phys. (2023), https://doi.org/10.1139/cjp-2023-0231.

[79] Z. M. Tang, Y. M. Yu, B. K. Sahoo, C. Z. Dong, Y. Yang, and Y. Zou, Phys. Rev. A **107**, 053111 (2023).

[80] M. A. Hohensee, N. Leefer, D. Budker, C. Harabati, V. A. Dzuba, and V. V. Flambaum, Phys. Rev. Lett. **111**, 050401 (2013).

[81] R. Shaniv, R. Ozeri, M. S. Safronova, S. G. Porsev, V. A. Dzuba, V. V. Flambaum, and H. Häffner, Phys. Rev. Lett. **120**, 103202 (2018).

[82] V. A. Dzuba, V. V. Flambaum, M. S. Safronova *et al.*, Nat. Phys. **12**, 465 (2016).

[83] B. K. Sahoo, Phys. Rev. A **99**, 050501(R) (2019).

[84] Y. Huang, H. Guan, C. Li, H. Zhang, B. Zhang, M. Wang, L. Tang, T. Shi, and K. Gao, arXiv:2202.07828v1.

[85] V. A. Dzuba and V. V. Flambaum, Phys. Rev. A **108**, 053111 (2023).

[86] P. Dubé, A. A. Madej, Z. Zhou, and J. E. Bernard, Phys. Rev. A **87**, 023806 (2013).

[87] A. Derevianko, V. A. Dzuba, and V. V. Flambaum, Phys. Rev. Lett. **109**, 180801 (2012).